Surface crack growth in metallic pipes reinforced with Fibre-Reinforced Polymers subjected to cyclic loads

An analytical approach

Li, Zongchen; Jiang, Xiaoli; Hopman, Hans; Affolter, Christian

DOI
10.1016/j.tafmec.2023.104070

Publication date
2023

Document Version
Final published version

Published in
Theoretical and Applied Fracture Mechanics

Theoretical and Applied Fracture Mechanics 127 (2023) 104070

Contents lists available at ScienceDirect

Theoretical and Applied Fracture Mechanics

journal homepage: www.elsevier.com/locate/tafmec

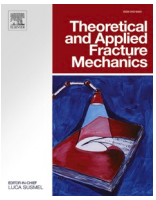

Surface crack growth in metallic pipes reinforced with Fibre-Reinforced Polymers subjected to cyclic loads: An analytical approach

Zongchen Li [a,b,*], Xiaoli Jiang [a], Hans Hopman [a], Christian Affolter [b]

[a] Department of Maritime and Transport Technology, Delft University of Technology, 2628 CD Delft, the Netherlands
[b] Mechanical Systems Engineering, EMPA-Swiss Federal Laboratories for Materials Science and Technology, 8600 Duebendorf, Switzerland

ARTICLE INFO

Keywords:
Surface crack growth
Fibre-Reinforced Polymer reinforcement
Crack-bridging effect
Interfacial stiffness degradation
Interfacial fatigue damage
Cohesive zone model

ABSTRACT

This paper introduces a novel analytical approach aimed at predicting the growth of surface cracks in metallic pipes reinforced with Fibre-Reinforced Polymers (FRPs) subjected to cyclic bending and/or tension loads. The primary objective of this study is to develop a comprehensive analytical model that accounts for multiple factors influencing crack growth, namely stress reduction, crack-bridging effect, stiffness degradation, and fatigue damage of the FRP-to-metal interface simultaneously. By considering these simultaneous effects, our proposed approach enables accurate evaluations of the stress intensity factors (SIFs) at both the surface point and the deepest point of a surface crack. To facilitate practical implementation, we have developed an in-house program that automates crack growth rate and residual fatigue life predictions. The proposed analytical method has been validated through a series of comparisons with experimental data and finite element results, demonstrating its accuracy in estimating fatigue lives. The key novelties of this research lie in the holistic consideration of multiple dominating and influencing factors, the achievement of precise SIF evaluations, and the development of an automated prediction tool for practical applications. Overall, our findings confirm the suitability of the proposed analytical approach for predicting crack growth and provide valuable insights for guiding the design of FRP reinforcement in surface-cracked metallic pipes. This work contributes to advancing the understanding of crack growth behaviour in FRP-reinforced metallic pipes and opens new possibilities for the safe and efficient design of such structures.

1. Introduction

Fibre-Reinforced Polymers (FRPs) have been extensively applied for repairing damaged metallic pipes for decades, known as the Composite Repair System in the piping industry [1]. In the past decade, research has elucidated the efficacy of FRPs in repairing pipes with corrosion [2,3], holes or defects [4–7], and cracks [2,8–13]. Both FRP wrappings and patches, utilizing either Carbon-FRP or Glass-FRP, have been employed to ascertain the post-repair failure pressure [7,14], stress intensity factor [2,9,10,12,13] or the J-integral [8,15] associated with the crack.

In contrast to those pipelines exposed to internal pressure, offshore metallic pipes, including risers, are subjected to sustained dynamic forces due to oceanic waves, winds, currents, and second-order floater motions [16]. Notably, these pipelines maintain a near-equilibrium between internal and external pressures. These dynamic forces result in significant cyclic axial stresses, manifesting as tension and/or bending on the pipeline. Consequently, this can induce the initiation and propagation of surface cracks, culminating in potential leakages or fractures.

Repairing surface cracks prevent or postpone pipe leakage in advance. The aforementioned literature on repairing cracked pipes mainly focused through-thickness cracks, whereas repairing surface cracks, which has an approximately semi-elliptical crack front, needs more attention on crack propagation on both along the crack length direction and the crack depth direction. Our previous studies have employed experimental and finite element approaches to investigate surface crack growth in metallic pipes reinforced with FRP [17–19]. The experimental studies proved the efficiency of FRP reinforcement [17]. In addition, the experimental results of the crack growth rate indicate the crack-bridging effect might play a secondary role on the reinforcement efficiency. The three-dimensional finite element studies provided an effective approach for predicting crack growth rate and residual fatigue life [18,19]. In addition, the crack-bridging effect of reinforcing external defects has been further confirmed, and the FRP-to-steel interfacial stiffness degradation has been observed. Moreover, critical influential

* Corresponding author.
E-mail address: zongchen.li@empa.ch (Z. Li).

https://doi.org/10.1016/j.tafmec.2023.104070
Received 1 June 2023; Received in revised form 28 August 2023; Accepted 29 August 2023
Available online 29 August 2023

Nomenclature

A_i	the cross-section area of each layer in a FRP reinforced pipe
a	crack depth of a surface crack
a_0	depth of a semi-elliptical crack notch
a/c	aspect ratio of a surface crack
C	curvature of a pipe under bending
C_A, m_A	Paris' law constants for the deepest point of a surface crack
C_B, m_B	Paris' law constants for the surface point of a surface crack
c	half crack length of a surface crack
c_0	half-length of a semi-elliptical crack notch
D_p	external diameter of the pipe
d_p	internal diameter of the pipe
E_a	elastic modulus of the adhesive
E_p	elastic modulus of a metal pipe
E_i	elastic modulus of layer i along the normal direction
$E_{i,\,eff}$	effective elastic modulus of a fibre layer
F	boundary correction factor of evaluating Stress Intensity Factor (SIF)
F_i	total tensile force of each layer in the FRP reinforced pipe
F_{total}	total tensile force applied on a FRP reinforced pipe
G	bending correction factor by considering stress gradient effect
I_i	second moment of area of layer i
L	pipe length
L_i, L_e	inner span and external span of the 4-point bending test setup
$M_{b,total}$	total bending moment
$M_{b,i}$	bending moment of each layer i
$M_{b,p}$	bending moment shared by a metal pipe
ΔN	cycle increment
Q	approximation factor of evaluating SIF
t	thickness of a pipe
t_a	thickness of the adhesive layer at the FRP-to-metal interface
R	stress ratio
R_i, r_i	external and internal radius of layer i
R_p, r_p	external and internal radius of a pipe
K_I	Mode-I stress intensity factor
$K_{I,A}$	SIF at the deepest point of a surface crack
$K_{I,B}$	SIF at the surface point of a surface crack
k_1, k_2, b_2	slope and the y-value for a bi-linear traction-separation law
V_f	fibre volumetric fraction
σ_0	maximum traction stress of the traction-separation law
σ_c	traction stress of traction-separation law
σ_i, ε	normal stress and strain in each layer in a FRP reinforced pipe
σ_p	normal stress distributed in a pipe
$\sigma_{p,c}$	normal stress distributed in a pipe when considering the traction stress
$\sigma_{p,t}$	normal stress distributed in a pipe subjected to tension
$\sigma_{p,b}$	normal stress distributed in a pipe subjected to bending
$\sigma_{p,b,\,max}$	maximum normal stress distributed in a pipe subjected to bending
σ_y	yield strength of metal substrate
φ	the eccentric angle of a surface crack
φ_c	the eccentric angle for the surface point of a surface crack
$\Delta\sigma_0$	increment of damage at the FRP-to-metal interface
ε_s	maximum principle strain
ε_{th}	the threshold strain
δ	maximum separation of the traction-separation law
δ_0	the separation when the traction stress reaches the maximum
δ_c	the real-time separation in the traction-separation law
θ	angle between the fibre orientation and the principle stress

parameters in terms of cracks and pipe geometries, and reinforcement schemes have been discussed.

High financial and time cost, as well as high requirements of user expertise have restricted the application of experimental and finite element approaches in practice. A reliable analytical approach owns considerable value by virtue of its user-friendly feature, high efficiency, and rational accuracy. In addition, neat formulas within an analytical approach enable users to intuitionally comprehend its mechanism and to quantify each parameter. Previous studies that focused on analytical approaches have made good attempts to predict crack growth in metallic components reinforced with FRP. Wang and Rose [20] proposed a crack bridging model to calculate the stress intensity factor (SIF) of central cracks in plates with a one-side bonded patch. Liu, et al. [21] conducted a theoretical study of the central-crack growth in Carbon-FRP (CFRP) repaired steel plates through the analysis of the strain distribution in the FRP layers and the stress distribution at the cracked section. Semi-analytical methods by combing finite element analysis (FEA) to determine correction factors for the analytical approach were proposed in the past decade as well. Yu, et al. [22] used linear-elastic fracture mechanics (LEFM) to evaluate the Stress Intensity Factor (SIF) at crack tips of CFRP bonded steel plates, where FEA was adopted to calculate the geometry correction factor, so did the study by Wang, et al. [23] on the SIF of double-edged cracks. To the present, we are aware of the fact that the effectiveness of FRP reinforcement in reducing crack growth rate owes to the decreasing stress field and the crack-bridging effect when FRP laminates contact the cracked surface [17,19].

The crack-bridging effect on decreasing crack growth rate may not be simply presented as a constant value. With further comprehension of adhesive bonding mechanism, researchers realized the importance of interfacial bond behaviour [24,25]—debonding failure could reduce the reinforcement efficiency. This is in general known as the crack-induced debonding [24] or stiffness degradation [19] in the scenario of using FRP to repair cracked structures, usually considered via the cohesive zone model (CZM) [26–28]. The traction-separation law, on which the CZM is based, is adequate for reinforced structures under static or monotonic loads. However, it is insufficient for cases under cyclic loads since the bond interface could suffer from fatigue damage simultaneously [29]. Therefore, when analysing crack growth in metallic structures reinforced with FRP under cyclic loads, interfacial fatigue damage shall be integrated into the traction-separation law. Hence, a real-time crack-bridging effect on crack growth can be rationally considered.

The utilization of FRP for repairing surface cracks in metallic pipes presents unique challenges, distinguishing it from the repair of through-thickness cracks typically encountered in other scenarios [16]. Furthermore, the cylindrical geometry and specific load conditions of pipes introduce further distinctions compared to cracks in flat plates. In light of these considerations, this paper presents a novel analytical approach to predict the growth of surface cracks in metallic pipes reinforced with FRP subjected to cyclic axial loads. The critical dominating and influential parameters, including the stress reduction, the crack-bridging effect along with stiffness degradation or crack-induced debonding, and fatigue damage at the FRP-to-metal interface, are considered in the approach simultaneously, in order to ensure an accurate prediction on the crack propagation. Following the Introduction, Section 2 introduces and discusses the methodologies that have been utilised. Section 3 establishes the analytical approach. The validity of the approach is then demonstrated through fatigue experimental

investigations and numerical results in Section 4. Finally, the conclusions are presented in Section 5.

2. Methodology of the analytical approach

Based on insights from previous studies, it has been established that the reinforcement effect in surface-cracked pipes is primarily attributed to stress reduction near the cracks and the crack-bridging effect of external reinforcement [17,19]. However, it is important to acknowledge that the presence of high regional deformation may weaken the crack-bridging effect, which must be duly considered in the analytical approach. In this section, we present the methodology of our proposed approach, highlighting key aspects such as stress degradation adjacent to cracks, the crack-bridging effect, stiffness degradation, and fatigue damage at the FRP-to-metal interface. In essence, the FRP reinforcement alters the boundary conditions of the surface crack's propagation within pipes by modifying the stress distribution and introducing the crack-bridging effect.

2.1. Stress reduction owing to FRP reinforcement

In the case of reinforced pipes subjected to tension, the methodology for calculating the shared load by the pipe involves considering that all layers, including the metallic pipe, FRP layers, and adhesive layers, share the same normal strain. This is illustrated in Fig. 1 in the Y-Z cutting plane. Consequently, the shared stress borne by the pipe can be readily determined. It is important to note that for the sake of simplification in calculations, only the stiffness along the direction of tension is taken into account.

In contrast to pipes under tension, the layers within FRP-reinforced pipes subjected to bending do not share the same strain. Instead, each layer, resembling a hollow cylinder, experiences the same curvature. This is depicted in Fig. 2 in the Y-Z cutting plane. Consequently, by evaluating the overall curvature, considering the total applied bending moment and the equivalent stiffness of the entire reinforced structure, the bending moment borne by the metallic pipe can be determined. Subsequently, the normal stress within the pipe adjacent to a surface crack can be computed.

2.2. Crack-bridging effect on the surface point of a crack

In the context of circumferential surface cracks in a metallic pipe (see in Fig. 3), they typically exhibit a semi-elliptical shape characterized by the crack faces and the semi-elliptical crack front. As shown in Fig. 4. The most crucial points along the crack front are the surface points (B_1 and B_2) and the deepest point (A), as they play a significant role in determining the crack profile, propagation rate, and path. The crack-bridging effect specifically impacts the growth of the surface crack in the longitudinal direction (X-axis). It functions as a series of distributed springs connecting the crack faces at both ends, thereby imposing a closure force on the crack tip opening displacement (CTOD) at the surface points [30,31].

It is important to note that this paper primarily focuses on the crack-bridging effect at the surface points of the surface crack, where the CTOD represents the crack opening value infinitesimally close to these points. Consequently, the CTOD is equivalent to the separation at the FRP-to-metal interface. In the case of LEFM, the CTOD and SIF at the surface point can be interrelated. By incorporating the traction stress at the surface point into an equation, the SIF at that location can be determined. However, it should be emphasized that the traction stress at the deepest point is not considered since the FRP laminates do not make contact with it. Furthermore, it is important to acknowledge that the traction stress is not constant, as it is governed by interfacial properties and influenced by fatigue damage within the interface, which will be further discussed in subsections 2.2.1 and 2.2.2.

2.2.1. FRP-to-metal interfacial bond condition

A CZM is applied to consider the FRP-to-metal interfacial bond condition. When a pipe is under tension and/or bending, the FRP-to-metal interfacial traction stress is pre-dominated; therefore, a bi-linear traction-separation law is employed, as shown in Fig. 5. At the first stage along the bi-linear curve, the traction stress σ_c increases with the rising of the separation, while σ_c reaches the maximum value of σ_0 when the separation gets to δ_0. After that, the traction stress decreases gradually along the further increase of the separation value, known as stiffness degradation. Eventually, the traction stress completely disappears when the separation reaches the maximum δ, indicating the occurrence of debonding failure when the crack-bridging effect completely loses its effectiveness on the crack opening at the surface point.

2.2.2. Fatigue damage of the FRP-to-metal interface under cyclic loads

In the case of implementing FRP reinforcement under cyclic loads, fatigue damage in the FRP-to-metal interface shall be considered. In this paper, the FRP-to-metal interfacial fatigue damage is represented by the decreasing of traction stress, which is a function of cyclic numbers, governed by the bi-linear traction separation law [29], as shown in Fig. 5. To better understand, initially the maximum traction stress is σ_0, while it will decrease to $\sigma_{0,i}$ when the cyclic number N reaches i. Eventually, the maximum traction stress reaches zero after a certain number of cycles, indicating a complete fatigue failure at the FRP-to-metal interface.

It is important to highlight that the analysis of fatigue damage at the FRP-to-metal interface focuses solely on the vicinity of the cracked zone, as this area experiences significant localized deformation. Other regions of the interface do not undergo fatigue damage because the separation values (as depicted in Fig. 5) in those areas are much smaller than the threshold value.

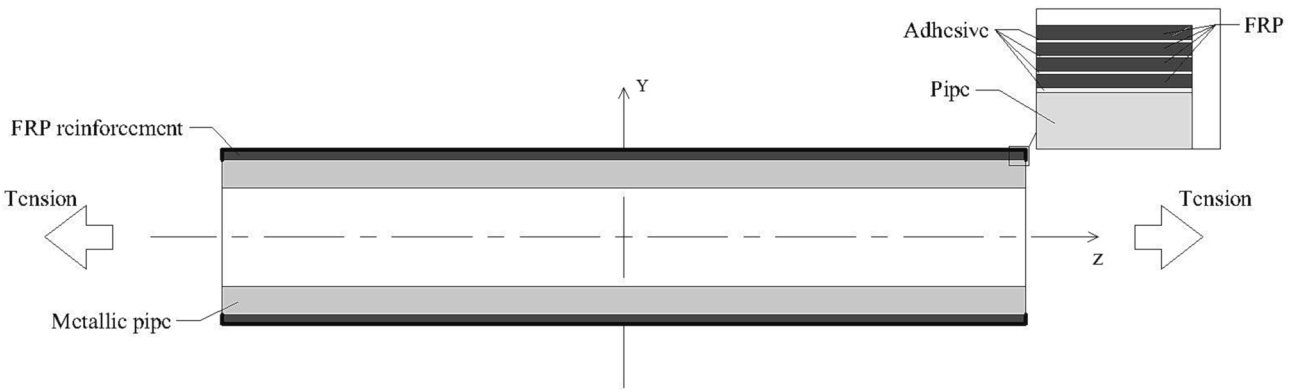

Fig. 1. Reinforced pipe under tension.

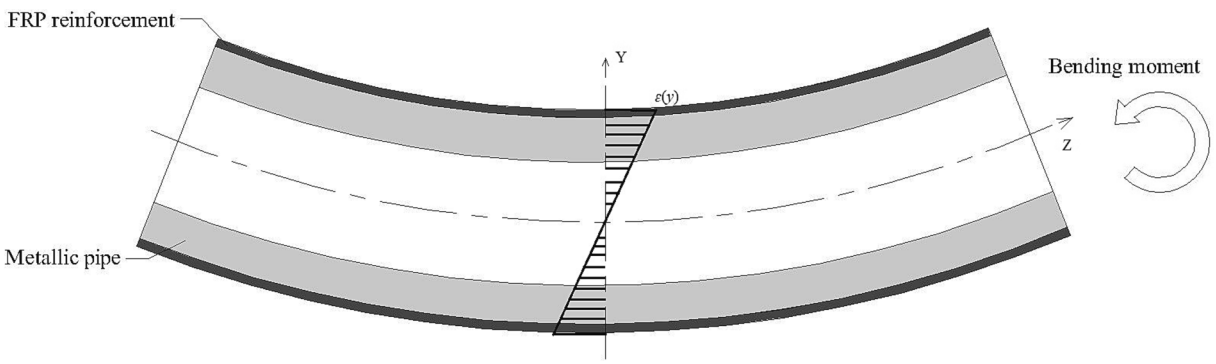

Fig. 2. Reinforced pipe under bending.

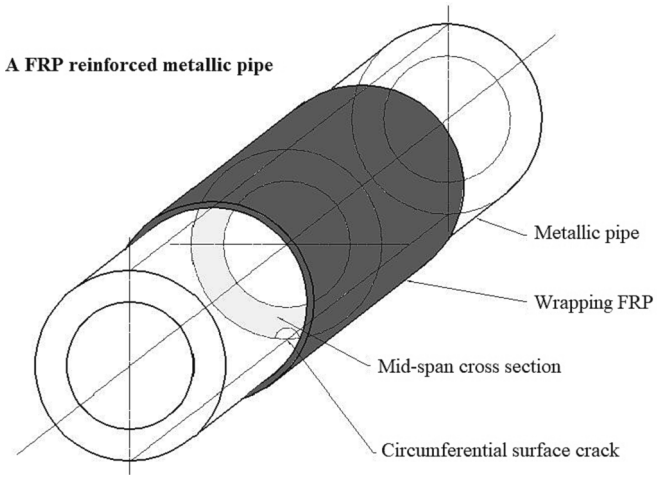

Fig. 3. FRP reinforced circumferential external surface cracked pipes in a metallic pipe.

The methodologies described above provide a solution for determining the applied stress field and the crack-bridging effect at the surface point. To calculate the SIF at the surface point, the two near-field stresses can be superimposed and integrated into the analytical approach proposed in our previous publication [16]. This approach allows for an accurate estimation of the SIF, taking into account the combined effects of the stress field and the crack-bridging effect.

3. The analytical approach to calculate SIFs

Building upon the methodology outlined in Section 2, this section presents the deduced and proposed analytical approach. The first step involves calculating the stress distribution in a FRP-reinforced pipe, considering various load cases such as tension, bending, or combined

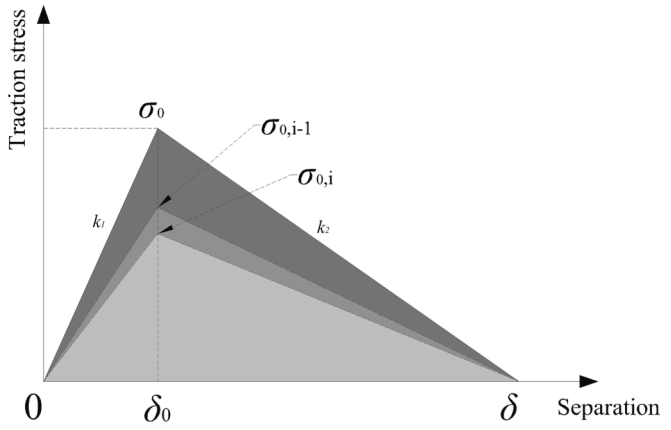

Fig. 5. The bi-linear traction-separation law and fatigue damage of the adhesive.

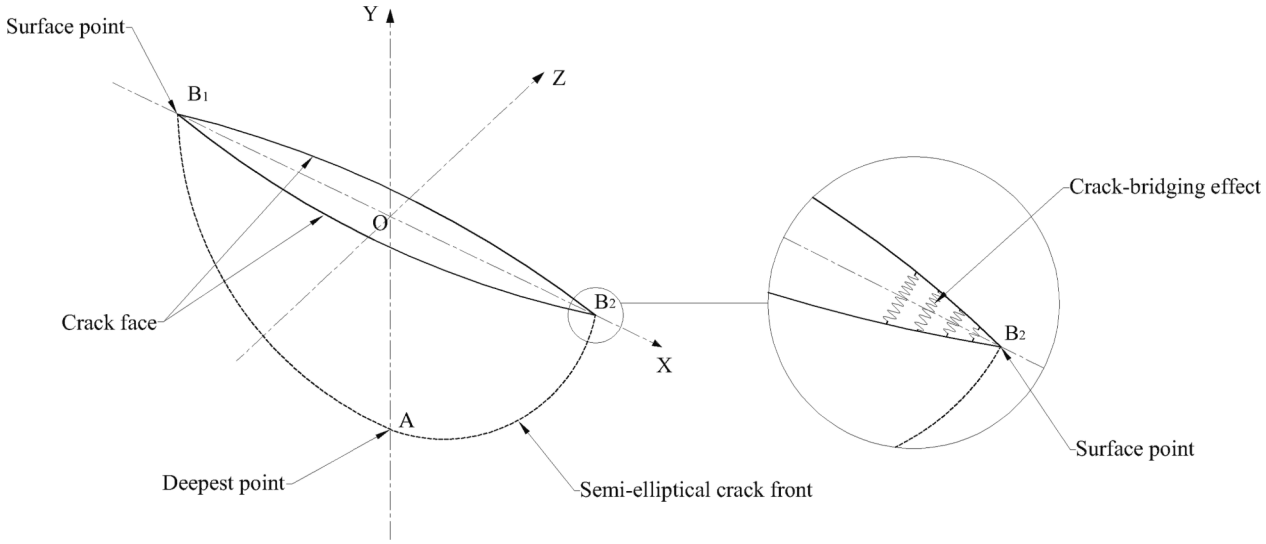

Fig. 4. A semi-elliptical surface crack and crack-bridging effect on the crack tip at the surface point.

loads. Next, recognizing the distinction between internal surface cracks and external surface cracks in terms of their location and the crack-bridging effect, we proceed to propose the analytical approach for internal surface crack growth. Subsequently, we present the approach specifically designed for external surface cracks.

3.1. Stress distributed in a pipe reinforced with FRP

a. Reinforced pipe subjected to tension.

When a FRP reinforced pipe is subjected to tension, the total tensile force equals to the sum of the tensile force shared by each layer, which is

$$F_{\text{total}} = \sum F_i, \tag{1}$$

where F_{total} is the total tensile force, F_i is the tensile force of each layer, which can be calculated as

$$F_i = \sigma_i \bullet A_i = E_i \bullet \varepsilon \bullet A_i, \tag{2}$$

where σ_i, ε, A_i, E_i are the normal stress, normal strain, cross-section area, and the elastic modulus along the normal direction of each layer, respectively. Hence the stress distributed within a pipe reinforced with FRP subjected to tension, $\sigma_{\text{p,t}}$, can be calculated as

$$\sigma_{\text{p,t}} = E_{\text{p}} \bullet \frac{F_{\text{total}}}{\sum E_i \bullet A_i}. \tag{3}$$

where E_{p} is the elastic modulus of a pipe.

Taking into account that the primary contribution to the reinforcement is the elastic modulus in the direction of the principal stress, only the component of the elastic modulus aligned with this principal stress direction is factored in. The Fibre volume friction has to be considered as well. Therefore, $E_{i,\text{ eff}}$ as the effective modulus of a fibre layer is used to replace the E_i for fibres, which is

$$E_{i,\text{ eff}} = E_i \bullet \theta \bullet V_f + E_a \bullet (1 - V_f), \tag{4}$$

where θ is the angle between the fibre orientation and the principle direction. V_f is the fibre volume fraction, and E_a is the elastic modulus of the adhesive. Note that the hoop-aligned portion of the elastic modulus won't directly reduce stress to reinforce, but it could enhance wrapping by adding stiffness.

b. Reinforced pipe subjected to bending moment.

When a FRP reinforced pipe is subjected to bending, the total bending moment $M_{\text{b,total}}$ equals to the sum of bending moment shared by each layer $M_{\text{b},i}$, as

$$M_{\text{b,total}} = \sum M_{\text{b},i}, \tag{5}$$

$$M_{\text{b},i} = C \bullet E_i \bullet I_i. \tag{6}$$

where C is the curvature of all layers. The $E_i \bullet I_i$ is the bending stiffness, where E_i is the elastic modulus of the layer i. Note the E_i for fibres with certain orientations should be replaced by the $E_{i,\text{ eff}}$ in Eq. (4) as well. I_i is the second moment of area, which is

$$I_i = \frac{\pi}{4} \bullet \left(R_i^4 - r_i^4\right). \tag{7}$$

where R_i and r_i are the external and internal radius of the layer i. Therefore, C is calculated as:

$$C = \frac{M_{\text{b,total}}}{\sum E_i \bullet I_i}. \tag{8}$$

Since all layers share the same curvature, the maximum bending moment shared by one individual layer can be calculated by Eq. (5). Then the normal bending stress of the steel pipe at the external surface along the longitudinal direction, $\sigma_{\text{p,b,max}}$, can be calculated as:

$$\sigma_{\text{p,b,max}} = M_{\text{b,p}} / \left[\frac{\pi \bullet R_{\text{p}}^3}{4} \bullet \left(1 - \frac{r_{\text{p}}^4}{R_{\text{p}}^4}\right)\right], \tag{9}$$

$$\sigma_{\text{p,b}} = G \bullet \sigma_{\text{p,b,max}}, \tag{10}$$

where $\sigma_{\text{p,b,max}}$ is the maximum stress when a pipe is subjected to bending, $M_{\text{b,p}}$ is the bending moment shared by the metallic pipe, R_{p}, r_{p} are the external and internal radius of the metallic pipe, $\sigma_{\text{p,b}}$ is the stress adjacent to a certain point along the surface crack front, G is the geometry correction factor when the pipe is subjected to bending [16]. For internal surface cracks,

$$G = \frac{2a \bullet \sin\varphi + d_{\text{p}}}{D_{\text{p}}}, \tag{11}$$

where a is the crack depth, D_{p} and d_{p} are the external- and internal diameter of a metal pipe, respectively. For external surface cracks,

$$G = \frac{D_{\text{p}} - 2a \bullet \sin\varphi}{D_{\text{p}}}, \tag{12}$$

where φ is the eccentric angle of a surface crack. The eccentric angle of the deepest point equals to $\pi/2$, while the eccentric angle of the surface point φ_c is calculate as

$$\varphi_c = \frac{\pi}{2} - \frac{\pi - \frac{c}{\frac{D_{\text{p}}}{2}}}{2} = \frac{c}{D_{\text{p}}}, \tag{13}$$

where c is the half crack length of a surface crack. In case the FRP reinforced pipe is subjected to tension and bending simultaneously, the overall normal stress distribute is calculated by Eq. (9) since they could be linearly superposed as

$$\sigma_{\text{p}} = \sigma_{\text{p,t}} + G \bullet \sigma_{\text{p,b,max}}. \tag{14}$$

3.2. SIF calculation

For scenarios of either a surface crack located at the internal surface of a pipe or at the external surface, the difference of the approaches lies in whether to consider the crack-bridging effect. Here we deduce the analytical approaches for internal-/external surface cracks separately.

a. Internal surface crack.

For internal surface crack, the crack propagation is not directly affected by the crack-bridging effect, thus the SIF can be directly calculated by the equation in Ref. [16] as:

$$K_{\text{I}} = \sigma_{\text{p}} \bullet \sqrt{\pi \frac{a}{Q}} \bullet F, \tag{15}$$

where F and Q are correction factors, of which the details can be found in Ref. [16] and Ref. [32].

b. External surface crack.

Stress decreased by the crack-bridging effect needs to be considered when reinforcing external surface cracks. Hence, σ_{p} in Eq. (13) shall be amended as $\sigma_{\text{p,c}}$, which is

$$\sigma_{\text{p,c}} = \sigma_{\text{p}} - \sigma_c. \tag{16}$$

σ_c is the traction stress at the surface point owing to the crack-bridging effect. Thus the SIF at the surface point of the crack, K_{Ic}, is

$$K_{I,B} = \sigma_{p,c} \bullet \sqrt{\pi \frac{a}{Q}} \bullet F. \tag{17}$$

In addition, stiffness degradation at the composite-to-steel interface has to be considered. The σ_c can be regard as the traction stress is determined using the traction-separation law (see in Fig. 5),

$$\sigma_c = \begin{cases} k_1 \bullet \delta_c (\delta_c \le \delta_0) \\ k_2 \bullet \delta_c + b_2 (\delta_0 < \delta_c < \delta) \\ 0 (\delta_c \ge \delta) \end{cases}, \tag{18}$$

where k_1 and k_2 can be obtained from Fig. 5, as

$$k_1 = \frac{\sigma_0}{\delta_0}. \tag{19}$$

$$k_2 = \frac{-\sigma_0}{\delta - \delta_0}. \tag{20}$$

$$b_2 = \frac{\sigma_0 \bullet \delta}{\delta - \delta_0} \tag{21}$$

where δ and δ_0 are interfacial properties given by the traction-separation law.

In addition, the fatigue damage of the FRP-to-metal interface is considered in the traction-separation model to calculate the real-time maximum traction stress, as shown in Fig. 5. The decreasing rate of the maximum traction stress σ_0 is calculated as,

$$\frac{\Delta \sigma_0}{\Delta N} = \begin{cases} \alpha (\varepsilon_s - \varepsilon_{th})^{\beta}, \varepsilon_{max} > \varepsilon_{th} \\ 0, \varepsilon_{max} \le \varepsilon_{th} \end{cases}, \tag{22}$$

where $\Delta\sigma_0$ is the increment of fatigue damage, ΔN is the cycle increment. ε_{th} is the threshold strain meaning that the interfacial fatigue damage only occurs when ε_s is larger than ε_{th}. α and β are material constants. ε_s is the maximum principal strain in the cohesive element, as:

$$\varepsilon_s = \frac{\delta_c}{t_a}, \tag{23}$$

where t_a is the thickness of the adhesive layer at the FRP-to-metal interface. Since the local displacement at the crack tip is defined as the CTOD, which can be interconverted with the SIF under the plane stress condition [33], therefore

$$\delta_c = \mathrm{CTOD} = \frac{4K_{IB}^2}{\pi \bullet E_p \bullet \sigma_y}, \tag{24}$$

where E_p is the elastic modulus of a metal pipe.

Therefore, combing Eqs. (14–17),K_{IB} can be calculated as independent variable in a quadratic equation as one variable, as:

$$K_{I,B} = \begin{cases} (\sigma_p - k_1 \bullet \delta_c) \bullet \sqrt{\pi \frac{a}{Q}} \bullet F(\delta_c \le \delta_0) \\ \left[\sigma_p - k_2 \bullet \delta_c - b_2\right] \bullet \sqrt{\pi \frac{a}{Q}} \bullet F(\delta_0 < \delta_c < \delta) \\ \sigma_p \bullet \sqrt{\pi \frac{a}{Q}} \bullet F(\delta_c \ge \delta) \end{cases}. \tag{25}$$

Since the bridging effect does not affect the SIF at the deepest point of the surface crack,

$$K_{I,A} = \sigma_p \bullet \sqrt{\pi \frac{a}{Q}} \bullet F. \tag{26}$$

Then the SIF at the surface point and the at deepest point can be calculated via the analytical method in [16], with the re-defined σ_p.

3.3. Evaluation of the surface crack propagation and fatigue life

Based on the SIF calculation at the deepest point and the surface point by the analytical approach, the Paris law is utilized [20] to determine the crack growth rate. This law allows for the calculation of incremental changes in crack length and depth with each cyclic loading, thereby capturing the crack propagation process over time. For automated analysis, an in-house Python program has been developed, which employs an algorithm outlined in the flow chart depicted in Fig. 6. This program not only calculates the crack growth process but also provides visualizations of the real-time interfacial bond condition between the FRP and metal, as well as the interfacial fatigue damage.

4. Results and validation

This section employed available numerical and experimental results to validate the proposed analytical approach for reinforcing internal surface cracked pipes and external surface cracked pipes, respectively.

4.1. Validation on the analytical method of predicting the internal surface crack growth

Available crack propagation results obtained from the finite element method [18] are applied to validate the analytical approach of predicting internal surface crack growth in metallic pipes reinforced with FRP. The pipe has an external diameter and wall thickness of 102.0 mm and 12.7 mm, respectively. The initial size of the internal surface crack is $a = 3.0$ mm, $c = 6.0$ mm. The steel pipe has an elastic modulus of 200 GPa, reinforced with three layers of CFRP with the L-L-H wrapping pattern (see in Fig. 7). Each CFRP layer has a thickness of 0.6 mm and the adhesive between the steel pipe and the first layer CFRP is 0.35 mm. The CFRP uses a unidirectional type of which the elastic modulus along the fibre direction is 205 GPa, whereas along the transverse direction is 25 GPa. Elastic modulus of the adhesive is 2.86 GPa. A fibre volumetric fraction $V_f = 0.6$ has been applied for the reinforcement. A bending moment of 1.8543×10^7kN • m is applied on the reinforced pipe, and a stress ratio $R = 0.1$ for the fatigue crack propagation. Paris' constants of $C_A = C_B = 3.6 \times 10^{-10}$and $m_A = m_B = 3.72$ has been modified and used for calculating the crack propagation rate with the SIF unit of MPa/$\mathrm{mm}^{1/2}$. Please refer to Ref. [18] for detailed information of the finite element analysis and results.

The comparison between the results shown in Fig. 8 indicates the analytical approach is able to deliver as accurate predictions as the numerical approach, which has been validated through the experimental results [34,35]. Eventually, the analytical approach predicts a total residual fatigue life of 434,123 cycles, with only a 1.21% error compared to the 439,448 cycles predicted by the numerical approach. When the crack penetrated the pipe wall, the analytical approach predicts a half crack length of 13.52 mm, with a 10% error to the result predicted by the numerical approach. The difference is because the crack propagation rate has been sharply increased owing to the significantly decreased net section area, which can be simulated via the numerical approach, while was not considered in the analytical approach.

4.2. Validation on the analytical approach of predicting the external surface crack growth

In this subsection, we validate the analytical approach of predicting the SIF and external surface crack growth, by conducting experimental investigations. The obtained results, as well as previous FEA results from the surface crack growth measurements in the experimental setup are compared with the predictions from the analytical approach, providing a comprehensive validation of the proposed methodology.

4.2.1. Experimental investigations

The sketch diagram of the FRP reinforced cracked specimen is shown in Fig. 9a, and the dimensions of the specimens are listed in Table 1, including the pipe length $L = 2{,}000$ mm, pipe external diameter $D_p =$

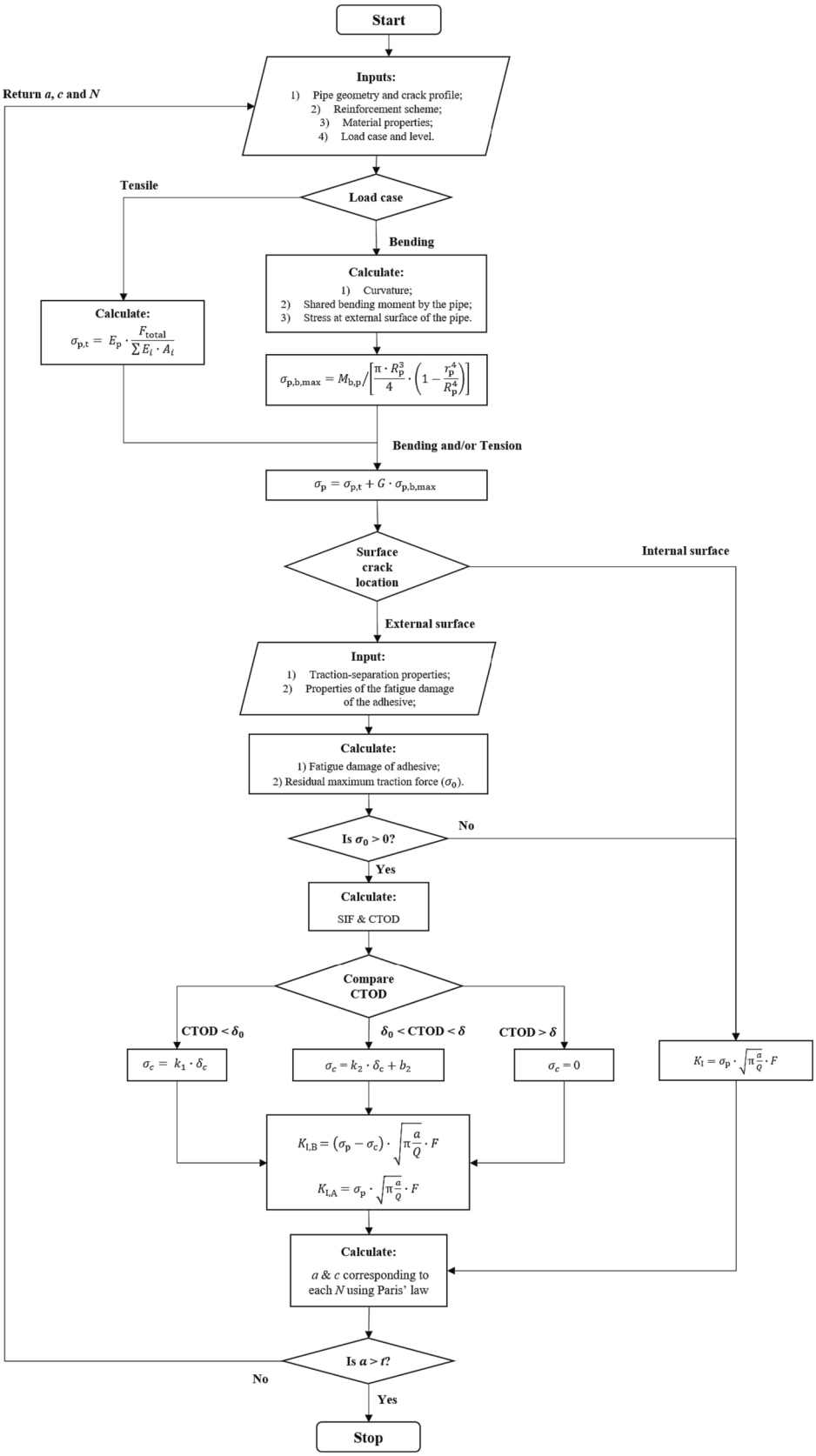

Fig. 6. Algorithm of the analytical approach.

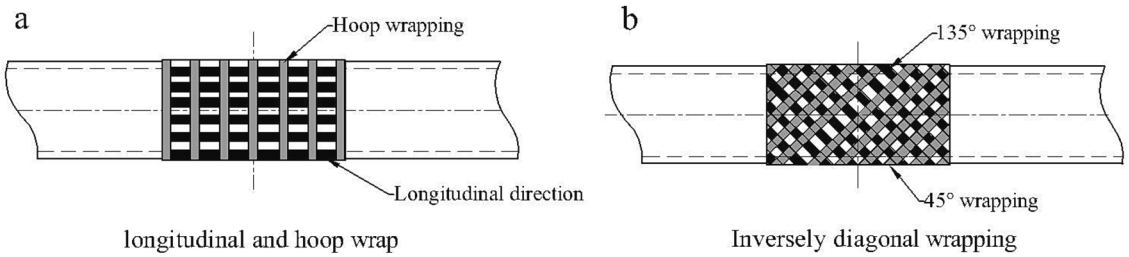

Fig. 7. Wrapping pattern: a) longitudinal (L) and hoop wrapping (H) pattern; b) inversely diagonal wrapping pattern $\theta = 45^{\circ}$

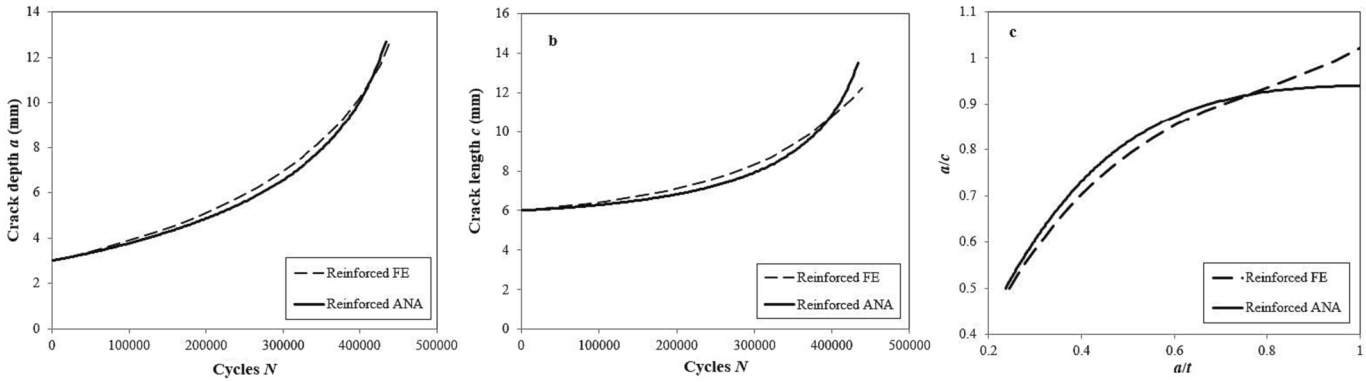

Fig. 8. The comparison of analytical results and finite element results for internal surface crack growth using three layers of CFRP: a) crack growth along the depth direction; b) crack growth along the length direction; c) aspect ratio variation with the crack growth. Note that 'ANA' stands for the analytical approach.

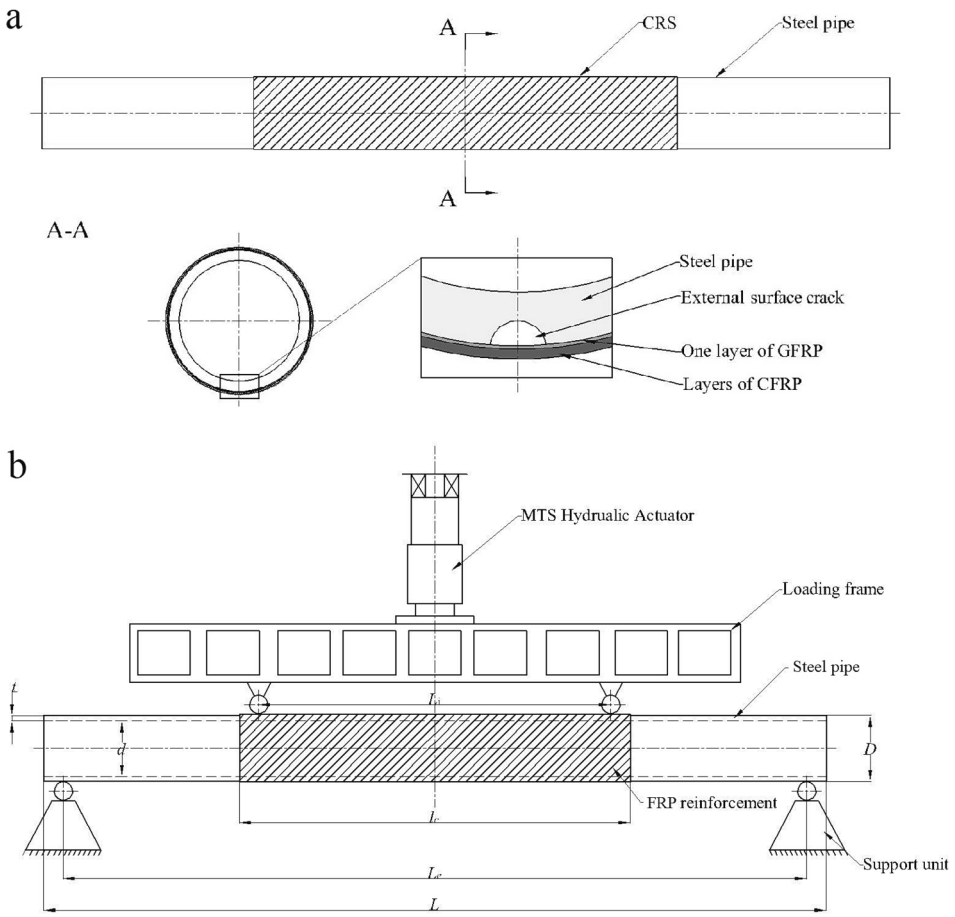

Fig. 9. a) The configuration of FRP reinforced steep pipe specimens; b) The schematic of the four-point bending test set-up.

168.3 mm, wall thickness of the pipe specimens $t = 12.7$ mm.

Semi-elliptical surface notches were pre-manufactured to initiate fatigue cracks with depth a_0 and half-length c_0 approximately equals to 2.5 mm and 5.0 mm. The steel pipe has an elastic modulus of 206 GPa and a yield strength of 448 MPa. The thickness of each layer of glass-FRP (GFRP) and CFRP laminate are 0.35 mm. The elastic modulus of the GFRP, CFRP, and the adhesive layer are listed in Table 2. In total, three groups of nine specimens were prepared, as listed in Table 1. Groups R1 to R3 are the FRP reinforcement groups with different reinforcement schemes. Details of the pipes' configuration and reinforcement schemes are summarized in Table 1. The name of the specimens represents the crack category, FRP reinforcement scheme, CFRP wrapping pattern, and their repetitive number. Take 'PE-1-R(1)' as an example, 'P' means steel pipe, 'E' represents external surface crack, the '1' stands for the crack category which are all '1' in this study, R means reinforcement, and the '(1)' means the No. of the repetitive specimen.

Fatigue tests followed the code of ASTM E647 [36] have been conducted, under constant amplitude sinusoidal cyclic loading. The experiment setup is illustrated in Fig. 9b. The load was applied in four-point bending condition to ensure a pure bending statue around the cracked location within the inner span $L_i = 800$ mm. The external span L_e is designed as 1,800 mm, therefore leaving the bending arm equals to 500 mm.

All the fatigue tests were conducted at room temperature and air environment under load control condition. The amplitude of the applied force, namely 241.54 kN, produced a maximum stress value of 268.8 MPa, accounting for 60% of the yield strength of the steel substrate. The loading frequency was set as 2.5 Hz. The load ratio R maintained 0.1 for the crack growth process of all tests. The crack growth process was recorded using beach marking technique by means of changing the load ratio R to 0.5 and cycled for 5,000 cycles.

Crack growth behaviour, i.e., the relation between the crack size and the cyclic numbers, was recorded by the beach marking technique. Then the crack sizes corresponding to each additional 10,000 cycles under $R = 0.1$ were measured by using an electronic reading microscope. The results are shown in Figs. 10-12, indicating the experimental results within each group matches each other very well with small scatters. For more information of the experimental results, Please refer to Ref. [17].

4.2.2. Validation by experimental results

Surface crack propagations of three scenarios, i.e., PE-1-R, PE-1-R8, and PE-1-R45 are calculated, added by an ANA suffix, such as PE-1-R ANA. The initial crack sizes for the analytical prediction use the crack size after the pre-cracking procedure from specimen PE-1-R(1), PE-1-R8 (1), and PE-1-R45(1). The material properties of the steel pipe, FRP, and adhesive, as well as wrapping schemes, keep in consist with the experimental specimens. A bi-linear traction-separation law has been assigned in the FRP-to-steel interface, with the maximum traction stress $\sigma_0 = 56.16$ MPa when the separation δ_0 reaches 0.011 mm. The maximum separation is $\delta = 0.16$mm. In addition, the fatigue damage parameters of the adhesive are $\alpha = 1.5$, $\beta = 2$, and $\varepsilon_{th} = 0.0319$ [29]. The thickness of each FRP layer is 0.35 mm and the thickness of the adhesive layer between the steel pipe and the GFRP is 0.2 mm, while the adhesive thickness between each FRP layer is 0.1 mm. A fibre volumetric fraction $V_f = 0.6$ has been applied for the reinforcement.

Table 2
The elastic modulus of FRP (along two in-plane directions) and adhesive [17].

Name	Elastic modulus (GPa)		
	1st direction	2nd direction	Fabrication
CFRP	230	25	Unidirectional
GFRP	72	72	0°-90° woven
Adhesive	3.4	/	/

A bending moment of 1.8543×10^7kN • m is applied on the pipes in the analytical approach which is identical to the fatigue test with the maximum applied load, with a stress ratio $R = 0.1$ to calculate the fatigue crack propagation rate. The Paris' constants are $C_A = 1.894 \times 10^{-15}$and $m_A = 3.664$ for crack growth along the depth direction, and $C_B = 8.462 \times 10^{-16}$ and $m_B = 3.785$ for along the length direction, with the SIF unit of MPa/mm$^{0.5}$, obtained from the experimental investigation [17]. The comparison between the analytical predictions and the experimental results are shown in Figs. 10-12.

The results shown in Figs. 10-12 clearly demonstrate that the analytical approach, which considered the crack-bridging effect (PE-1-R ANA), could accurately predict the surface crack growth in pipes reinforced with FRP subjected to cyclic bending. The predicted residual fatigue lives of PE-1-R, PE-1-R8, and PE-1-R45 have 2.75%, 1.67%, and 3.75% differences with respect to the experimental results. In addition, the analytical approach is able to capture the sharp increasing of crack propagation rate along the length direction owing to the FRP-to-steel bond failure, which also reproduces the turning point of the variation of the aspect ratios (a/c). Figs. 10-12 also include the prediction results of the analytical approach that did not consider the crack-bridging effect, represented in the dash lines (NTS, a.k.a. no traction stress, e.g., PE-1-R ANA NTS), which proposes far conservative predictions on crack propagation rate and residual fatigue life. Moreover, it could not capture the sharply increased crack propagation along the length direction, not to mention the aspect ratios variations. Please note the prediction results might be further improved, such as the mismatches of the a/c versus a/t curves between the analytical prediction and the experimental results in Figs. 10-12, by replacing the properties from formula derivation and literatures to data directly obtained from experiments.

The maximum traction stress (σ_0) marked with solid lines, and the real-time traction stress (σ_c) applied on the crack surface, marked with dash lines (named as "TS", a.k.a. traction stress, e.g., PE-1-R TS), with respect to the nominal crack length is shown in Fig. 13. The results demonstrate that the traction stress on PE-1-R8 which is reinforced with eight layers of CFRP, has the best performance in terms of the durability of the traction effectiveness. PE-1-R8 reached its maximum traction stress of 42.59 MPa when half the crack length ($c = 10.51$ mm) is 59.0% of final half the crack length ($c = 18.18$ mm) at failure, and the adhesive failed due to fatigue damage when the half crack length ($c = 14.53$ mm) reached 79.94 % of the final half crack length. Due to the lowest

Table 1
Specimens' configuration and reinforcement details.

Group	Specimen	Notch category	L (mm)	D_p (mm)	t (mm)	a_0 (mm)	c_0 (mm)	L_c (mm)	CFRP wrapping scheme
R1	PE-1-R(1)	1	2,000	168.3	12.63	2.31	4.94	1,000	L-L-L-H
	PE-1-R(2)	1	2,000	168.3	12.78	2.48	5.035	1,000	L-L-L-H
	PE-1-R(3)	1	2,000	168.3	12.76	2.44	4.885	1,000	L-L-L-H
R2	PE-1-R8(1)	1	2,000	168.3	12.77	2.56	5.09	1,000	L-L-L-H-L-L-L-H
	PE-1-R8(2)	1	2,000	168.3	12.72	2.56	4.90	1,000	L-L-L-H-L-L-L-H
	PE-1-R8(3)	1	2,000	168.3	12.63	2.48	5.15	1,000	L-L-L-H-L-L-L-H
R3	PE-1-R45(1)	1	2,000	168.3	12.74	2.46	4.95	1,000	Inversely diagonal
	PE-1-R45(2)	1	2,000	168.3	12.70	2.50	4.875	1,000	Inversely diagonal
	PE-1-R45(3)	1	2,000	168.3	12.79	2.52	4.87	1,000	Inversely diagonal

Note: The parameters, i.e., D_p, t, a_0, c_0 were measured based on each specimens, each of which is the weighted average of three measurement locations.

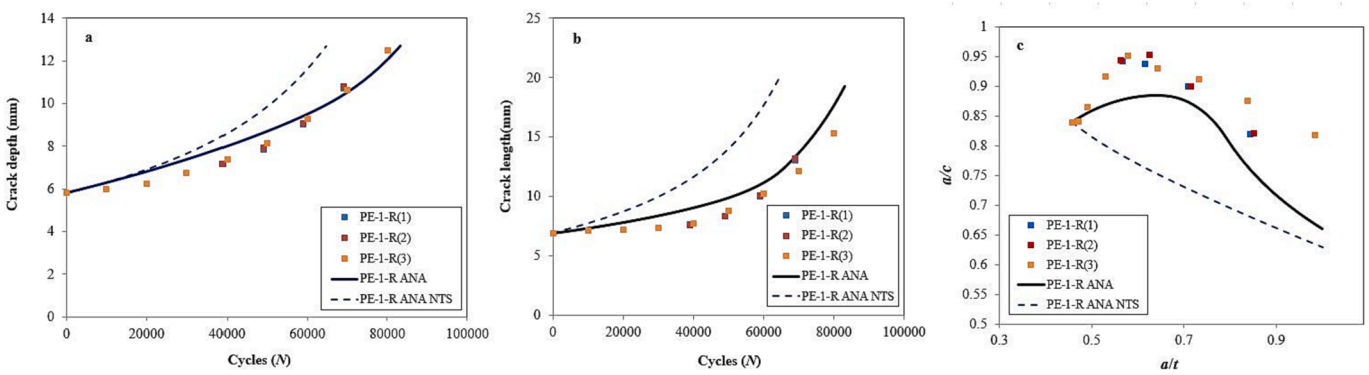

Fig. 10. The comparison of analytical results and experimental results for external surface crack growth using four layers CFRP: a) crack growth along the depth direction; b) crack growth along the length direction; c) aspect ratio variation with the crack growth.

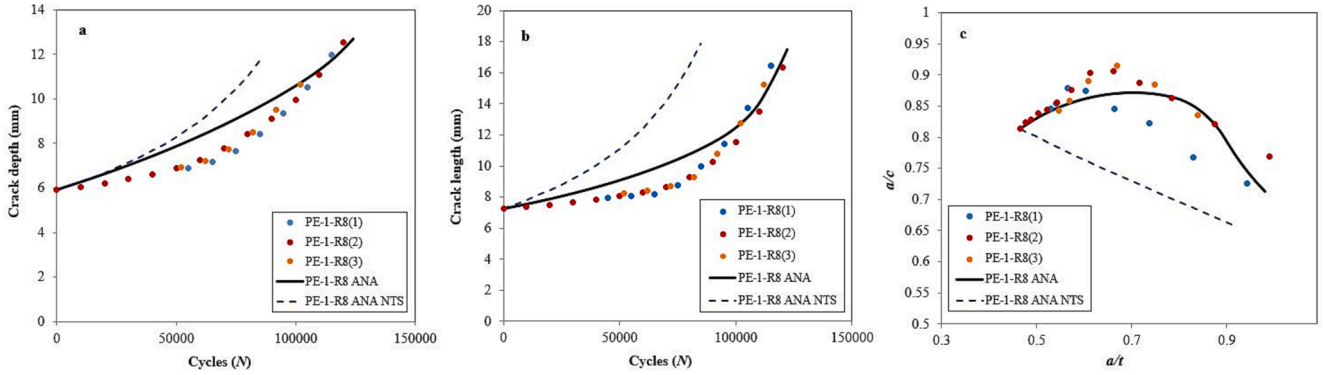

Fig. 11. The comparison of analytical results and experimental results of using eight layers of CFRP: a) crack growth along the depth direction; b) crack growth along the length direction; c) aspect ratio variation with the crack growth.

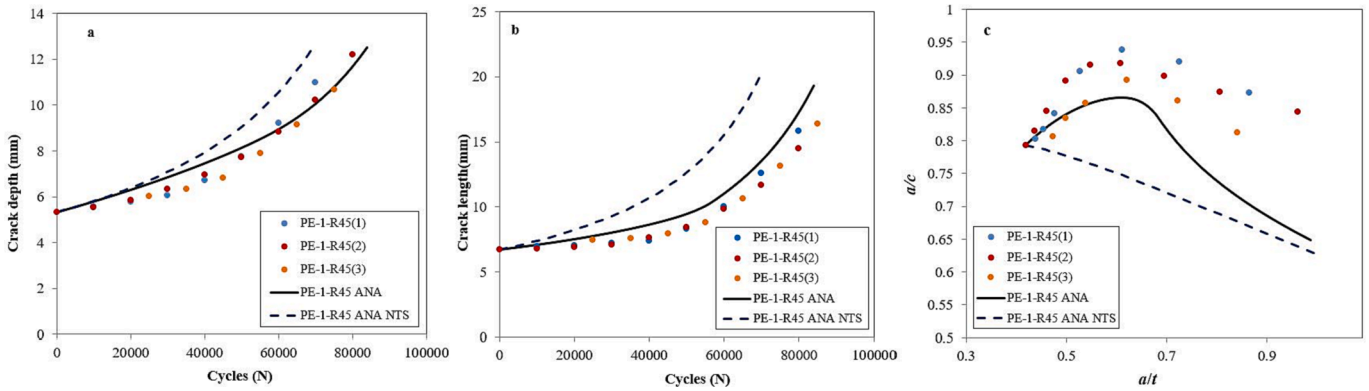

Fig. 12. The comparison of analytical results and experimental results for external surface crack growth of using the inversely diagnose wrapping pattern: a) crack growth along the depth direction; b) crack growth along the length direction; c) aspect ratio variation with the crack growth.

efficiency of FRP reinforcement, PE-1-R45 quickly reaches its peak of traction stress of 41.06 MPa at half the crack length of $c = 8.13$ (42.06% of the final half crack length), while quickly losing the traction at half the crack length of $c = 10.60$ mm (54.87% of final half the crack length). Therefore, we could infer that more efficient reinforcement schemes (e.g., applying more layers of CFRP, or using FRP with higher elastic modulus) would promote the effectiveness of the traction on the crack surface, which in return, would improve the overall reinforcement performance.

Furthermore, the ability of predicting surface crack growth in pipes with different dimensions (diameters and wall thicknesses) reinforced with FRP are investigated. Four different external diameters ranging from 168.3 mm to 323.8 mm with five different wall thicknesses from 10.97 mm to 21.95 mm are studied: five incremental pipe wall thickness has been discussed with $D_P = 168.3$ mm, while four incremental external diameter has been analysed with $t = 12.7$ mm. These dimensions are chosen owing to their frequently usage in the offshore piping industry. The applied longitudinal stress statue generated by the bending moment of all models is identical to the FEA, remaining at 268.8 MPa (60% of the yield strength).

The reduction in SIFs, which refers to the decrease in SIFs compared to the case of unreinforced surface cracks, is determined in this study. A crack size of $a = 5.98$ mm and $c = 7.12$ mm is employed for the analysis. The SIF reduction at the surface point (K_{IB}) resulting from the

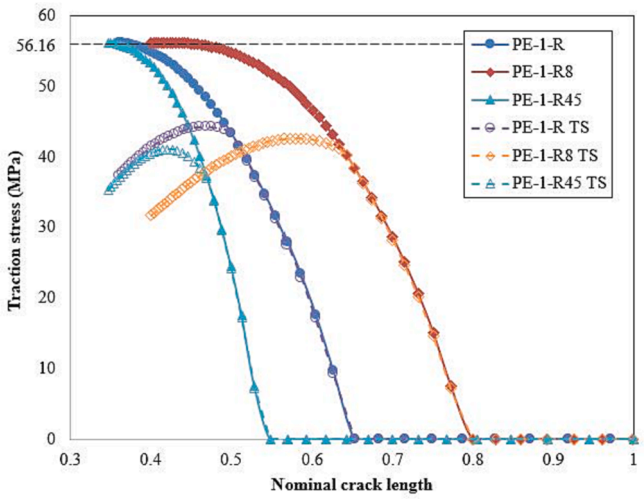

Fig. 13. Peeling stress on the three FRP reinforced models, predicted by the analytical approach.

introduction of FRP reinforcement using the same wrapping scheme as the PE-1-R model is calculated and compared with the available FEA results [19], as summarized in Table 3. The obtained results demonstrate a close agreement between the analytical predictions and the FEA predictions, with minor differences ranging from 0.4% to 5.7%. This validates the capability of the analytical approach to accurately predict SIFs in FRP-reinforced surface cracked pipes of various dimensions. The analytical approach serves as a reliable tool for assessing the effectiveness of FRP reinforcement in reducing SIFs in surface cracked pipes.

5. Conclusions

This paper presents a novel analytical approach aimed at predicting surface cracks growth in metallic pipes repaired using FRP composites subjected to cyclic bending and/or tensile loads. Critical factors including crack-bridging effect, stiffness degradation, and fatigue failure of the FRP-to-metal interface have been considered simultaneously, offering a comprehensive analysis of the crack growth phenomenon. The analytical approach demonstrates exceptional accuracy in forecasting surface crack growth, accommodating various pipe dimensions and wrapping schemes. It allows for a quantitative assessment of influential parameters pertaining to material properties, interfacial characteristics, and reinforcement strategies, providing valuable insights for designing FRP reinforcement in surface-cracked pipes. Consequently, its incorporation into pipe repair standards such as ASME PCC-2 [37] and BS EN ISO 24817:2015 [38] is highly recommended, as it offers a robust framework for guiding effective FRP reinforcement design and implementation, as well as offering an accurate evaluation on the post-repair residual fatigue life.

CRediT authorship contribution statement

Zongchen Li: Conceptualization, Methodology, Validation, Formal analysis, Data curation, Writing – original draft, Writing – review & editing, Visualization. **Xiaoli Jiang:** Conceptualization, Supervision. **Hans Hopman:** Supervision, Funding acquisition. **Christian Affolter:** Methodology, Writing – review & editing.

Declaration of Competing Interest

The authors declare that they have no known competing financial interests or personal relationships that could have appeared to influence the work reported in this paper.

Table 3
Configurations of steel pipe models with different dimensions, and the results of the SIF decrease.

Model No.	D_p (mm)	t (mm)	K_{IB} reduction (ANA)	K_{IB} reduction (FEA)	Difference between ANA and FEA
1	168.3	10.97	30.1%	29.5%	2.0%
2	168.3	12.70	27.7%	27.3%	1.5%
3	168.3	14.27	26.1%	26.0%	0.4%
4	168.3	18.26	23.6%	23.8%	0.8%
5	168.3	21.95	22.2%	22.6%	1.8%
6	219.1	12.70	26.9%	28.2%	4.6%
7	273.0	12.70	26.4%	25.3%	4.3%
8	323.8	12.70	26.0%	24.6%	5.7%

Data availability

Data will be made available on request.

Acknowledgement

The first author appreciate Laboratory for Mechanical Systems Engineering at Empa, Switzerland, and Department of Maritime and Transport Technology at Delft University of Technology, the Netherlands for supporting this research. The first author would like to acknowledge Dr Jian Zhang from Eindhoven University of Technology, the Netherlands for insightful discussions.

References

[1] N. Saeed, H. Ronagh, A. Virk, Composite repair of pipelines, considering the effect of live pressure-analytical and numerical models with respect to ISO/TS 24817 and ASME PCC-2, Compos. B Eng. 58 (2014) 605–610.
[2] M.A. Ghaffari, H. Hosseini-Toudeshky, Fatigue crack propagation analysis of repaired pipes with composite patch under cyclic pressure, Art no. 031402, Journal of Pressure Vessel Technology, Transactions of the ASME 135 (3) (2013), https://doi.org/10.1115/1.4023568.
[3] A.O. Brahim, I. Belaidi, S. Khatir, C. Le Thanh, S. Mirjalili, M.A. Wahab, Strength prediction of a steel pipe having a hemi-ellipsoidal corrosion defect repaired by GFRP composite patch using artificial neural network, Compos. Struct. 304 (2023), 116299.
[4] Z.A. Alsharif, Design model of damaged steel pipes for oil and gas industry using composite materials. Part II: Modeling, *Advanced Structured Materials* 54 (2014) 147–156, https://doi.org/10.1007/978-3-319-07383-5_12.
[5] I. Skarakis, G. Chatzopoulou, S.A. Karamanos, N.G. Tsouvalis, A.E. Pournara, CFRP Reinforcement and Repair of Steel Pipe Elbows Subjected to Severe Cyclic Loading, Art no. 051403, Journal of Pressure Vessel Technology, Transactions of the ASME 139 (5) (2017), https://doi.org/10.1115/1.4037198.
[6] J. Reis, A. Costa, H. da Costa Mattos, Repair of damage in pipes using bonded GFRP patches, Compos. Struct. 296 (2022), 115875.
[7] A. Saffar, A. Darvizeh, R. Ansari, A. Kazemi, M. Alitavoli, Prediction of Failure Pressure in Pipelines with Localized Defects Repaired by Composite Patches, *J. Fail. Anal. Prev.* 19 (6) (2019) 1801–1814, https://doi.org/10.1007/s11668-019-00781-0.
[8] A.A. Abd-Elhady, H.E.D.M. Sallam, I.M. Alarifi, R.A. Malik, T.M.A.A. El-Bagory, Investigation of fatigue crack propagation in steel pipeline repaired by glass fiber reinforced polymer, Art no. 112189, Compos. Struct. 242 (2020), https://doi.org/10.1016/j.compstruct.2020.112189.
[9] F. Benyahia, A. Albedah, B.B. Bouiadjra, Stress intensity factor for repaired circumferential cracks in pipe with bonded composite wrap, Art no. 041201, Journal of Pressure Vessel Technology, Transactions of the ASME 136 (4) (2014), https://doi.org/10.1115/1.4026022.
[10] D. Kong, P. Zhou, C. Li, B. Hong, G. Xian, Stress intensity factor of through-wall-cracked steel pipe wrapped with prestressed CFRP composites, Art no. 109218, Eng. Fract. Mech. 283 (2023), https://doi.org/10.1016/j.engfracmech.2023.109218.
[11] J.M. Linden, M. Köpple, D. Elder, A.G. Gibson, Fracture mechanics of crack propagation in composite repairs of steel pressure piping, *J. Reinf. Plast. Compos.* 33 (6) (2014) 526–532, https://doi.org/10.1177/0731684413500366.
[12] Z. Valadi, H. Bayesteh, S. Mohammadi, XFEM fracture analysis of cracked pipeline with and without FRP composite repairs, *Mech. Adv. Mater. Struct.* 27 (22) (2020) 1888–1899, https://doi.org/10.1080/15376494.2018.1529844.
[13] H. Zarrinzadeh, M.Z. Kabir, A. Deylami, Extended finite element fracture analysis of a cracked isotropic shell repaired by composite patch, *Fatigue Fract. Eng. Mater. Struct.* 39 (11) (2016) 1352–1365, https://doi.org/10.1111/ffe.12446.
[14] M. Belhamiani, D.E. Belhadri, W. Oudad, O. Mansouri, W.N. Bouzitouna, J integral computation and limit load analysis of bonded composite repair in cracked pipes

under pressure, *Frattura ed Integrita Strutturale* 13 (50) (2019) 623–637, https://doi.org/10.3221/IGF-ESIS.50.53.
[15] L. Wang, S. Song, H. Deng, K. Zhong, Finite-Element Analysis of Crack Arrest Properties of Fiber Reinforced Composites Application in Semi-Elliptical Cracked Pipelines, *Appl. Compos. Mater.* 25 (2) (2018) 321–334, https://doi.org/10.1007/s10443-017-9621-9.
[16] Z. Li, X. Jiang, H. Hopman, L. Zhu, Z. Liu, An investigation on the circumferential surface crack growth in steel pipes subjected to fatigue bending, Theor. Appl. Fract. Mech. 105 (2019), 102403.
[17] Z. Li, X. Jiang, H. Hopman, L. Zhu, Z. Liu, External surface cracked offshore steel pipes reinforced with composite repair system subjected to cyclic bending: An experimental investigation, Theor. Appl. Fract. Mech. 109 (2020), 102703.
[18] Z. Li, X. Jiang, H. Hopman, Numerical analysis on the SIF of internal surface cracks in steel pipes reinforced with CRS subjected to bending, Ships and Offshore Structures (2019) 1, https://doi.org/10.1080/17445302.2019.1702769.
[19] Z. Li, X. Jiang, H. Hopman, External surface cracked offshore pipes reinforced with composite repair system: A numerical analysis, Theor. Appl. Fract. Mech. 117 (2022), 103191.
[20] C.H. Wang, L.R.F. Rose, A crack bridging model for bonded plates subjected to tension and bending, Int. J. Solids Struct. 36 (13) (1999) 1985–2014, https://doi.org/10.1016/S0020-7683(98)00070-5.
[21] H. Liu, Z. Xiao, X.L. Zhao, R. Al-Mahaidi, Prediction of fatigue life for CFRP-strengthened steel plates, Thin-Walled Struct. 47 (10) (2009) 1069–1077, https://doi.org/10.1016/j.tws.2008.10.011.
[22] Q. Yu, X. Zhao, Z. Xiao, T. Chen, X. Gu, Evaluation of stress intensity factor for CFRP bonded steel plates, Adv. Struct. Eng. 17 (12) (2014) 1729–1746.
[23] H. Wang, G. Wu, Y. Pang, Theoretical and numerical study on stress intensity factors for FRP-strengthened steel plates with double-edged cracks, Sensors 18 (7) (2018) 2356.
[24] B. Zheng, M. Dawood, Fatigue crack growth analysis of steel elements reinforced with shape memory alloy (SMA)/fiber reinforced polymer (FRP) composite patches, Compos. Struct. 164 (2017) 158–169.
[25] H. Zarrinzadeh, M. Kabir, A. Deylami, Crack growth and debonding analysis of an aluminum pipe repaired by composite patch under fatigue loading, Thin-Walled Struct. 112 (2017) 140–148.
[26] G. Barenblatt, Equilibrium cracks formed on a brittle fracture, Dokl. Akad. Nauk SSSR 127 (1) (1959) 47–50.
[27] D.S. Dugdale, Yielding of steel sheets containing slits, J. Mech. Phys. Solids 8 (2) (1960) 100–104.
[28] G.I. Barenblatt, The mathematical theory of equilibrium cracks in brittle fracture, Adv. Appl. Mech. 7 (1962) 55–129.
[29] H. Khoramishad, A. Crocombe, K. Katnam, I. Ashcroft, Predicting fatigue damage in adhesively bonded joints using a cohesive zone model, Int. J. Fatigue 32 (7) (2010) 1146–1158.
[30] L.F. Rose, Crack reinforcement by distributed springs, J. Mech. Phys. Solids 35 (4) (1987) 383–405.
[31] V.D. Krstic, On the fracture of brittle-matrix/ductile-particle composites, Philos. Mag. A 48 (5) (1983) 695–708.
[32] J. Newman Jr and I. Raju, "Analysis of surface cracks in finite plates under tension or bending loads," 1979.
[33] T.L. Anderson, Fracture mechanics: fundamentals and applications, CRC Press, 2017.
[34] Y. Yoo, K. Ando, Circumferential inner fatigue crack growth and penetration behaviour in pipe subjected to a bending moment, Fatigue Fract. Eng. Mater. Struct. 23 (1) (2000) 1–8.
[35] M. Kabir, S. Fawzia, T. Chan, J. Gamage, J. Bai, Experimental and numerical investigation of the behaviour of CFRP strengthened CHS beams subjected to bending, Eng. Struct. 113 (2016) 160–173.
[36] ASTM, ASTM E647. Standard Test Method for Measurement of Fatigue Crack Growth Rates. 1994.
[37] ASME, *ASME PCC-2: Repair of Pressure Equipment and Piping*. American Society of Mechanical Engineers, 2015.
[38] BS, BS EN ISO 24817:2015. Petroleum, petrochemical and natural gas industries-Composite repairs for pipework-Qualification and design, installation, testing and inspection. British Standards Institution, 2015.